Jeught & Dirckx: Real-time Structured Light Profilometry: A Review

Friday, February 12, 2021 12:49 AM

vanderjeught2016

ARTICLE IN PRESS

Optics and Lasers in Engineering ■ (■■■■) ■■■–■■■

Contents lists available at ScienceDirect

Optics and Lasers in Engineering

journal homepage: www.elsevier.com/locate/optlaseng

Real-time structured light profilometry: a review

Sam Van der Jeught [a,*], Joris J.J. Dirckx [a]

[a] Laboratory of Biomedical Physics (BIMEF), University of Antwerp, Groenenborgerlaan 171, B-2020 Antwerp, Belgium

ARTICLE INFO

Article history:
Received 24 September 2015
Received in revised form
16 December 2015
Accepted 21 January 2016

Keywords:
Real-time
Structured light profilometry
Review
Phase unwrapping

ABSTRACT

The acquisition of high-resolution, real-time three-dimensional surface data of dynamically moving objects has large applicability in many fields. When additional restrictions such as non-invasiveness and non-contact measurement are imposed on the employed profilometry technique, the list of possible candidates is reduced mainly to the broad range of structured light profilometry methods. In this manuscript, the current state-of-the-art in structured light profilometry systems is described, as well as the main advancements in hardware technology and coding strategy that have led to their successful development. A chronological overview of optical profilometry systems that have been reported to perform real-time acquisition, digital signal processing and display of full-field 3D surface maps is presented. The respective operating principles, strengths and weaknesses of these setups are reviewed and the main limitations and future challenges in high-speed optical profilometry are discussed.

© 2016 Elsevier Ltd. All rights reserved.

1. Introduction

With recent technological advancements in digital projection, imaging and processing hardware, optical surface measurement techniques have evolved rapidly. The demand for non-contact, high-resolution and fast 3D-shape measurement systems is propelled by the medical, industrial and entertainment sector and has driven manufacturers and academic research groups to design a wide variety of optical profilometry techniques. Generally, they vary in terms of hardware configuration, stability, cost, resolution and speed.

Time-of-flight profilometers [1–3] measure the time required for a light pulse to travel from the transmitter to an object and back to the receiver. The object surface is scanned point-per-point in an array of arbitrarily dense sampling points and a depth map is created subsequently. Time-of-flight methods are generally stable, straightforward 3D-measurement techniques and require no calibration to produce absolute depth data. However, axial measurement accuracy (typically 0.1–1 cm) is limited to the temporal resolution of the transmitter-receiver system and cannot be improved through optical magnification.

Image-based techniques analyze how an image is formed and how lighting affects the objects within that image. Three-dimensional surface information is extracted from the two-dimensional representation of the object through (complicated) image analysis. *Shape-from-shading* methods [4,5] recover the surface shape from the image by modeling the gradual variations of grayscale shading in the image and by determining each pixel's relative distance to the imaging source. *Shape-from-focus-and-defocus* methods [6,7] recover the surface shape by correlating the degree of local blur on the object to relative distance from the imaging lens. *Stereo vision* profilometry techniques [8,9] simulate the stereoscopic setup of human vision by employing a second camera placed at an angle with the original camera. Identifying common features on the object in images taken from multiple perspectives or *stereo-matching* allows the object surface shape to be reconstructed using standard triangulation techniques. Image-based profilometry techniques require only a digital camera (or two, in the case of stereo vision techniques) and are generally low-cost setups. However, limited measurement accuracy in depth and computationally intensive digital signal processing requirements reduce their usability in real-time profilometric setups.

Similar to stereo-vision profilometry, *Moiré profilometry* [10,11] requires an additional optical axis in its setup design. By replacing one of the two cameras with a projection device to illuminate the object with structured light patterns, one can avoid the stereo-matching problem. When observed under an angle, the projected patterns are deformed by the object's surface shape. In Moiré profilometry, mechanical interference is induced by placing a demodulation grid - identical but slightly misaligned to the original projection grid - between the object and the camera. Contours of equal height can then be extracted from the resulting interference pattern. Practically, however, the need for a physical demodulation grid complicates the hardware configuration of the experimental setup.

* Corresponding author.
E-mail address: sam.vanderjeught@ua.ac.be (S. Van der Jeught).

http://dx.doi.org/10.1016/j.optlaseng.2016.01.011
0143-8166/© 2016 Elsevier Ltd. All rights reserved.

Please cite this article as: Van der Jeught S, Dirckx JJJ. Real-time structured light profilometry: a review. Opt Laser Eng (2016), http://dx.doi.org/10.1016/j.optlaseng.2016.01.011

More recently, various *structured light projection* (SLP) techniques have been reported that employ the same projector–camera setup as Moiré techniques but lack the demodulation grid. Instead, surface height information is extracted directly from analysis of the deformed grid pattern. By eliminating the demodulation grid, SLP techniques allow for a more straightforward and stable experimental setup to be designed. In addition, specific depth extraction can be performed in a number of ways, depending on the nature and the amount of projected patterns.

The remainder of the paper is structured as follows: in Section 2, the broad range of structured light profilometry techniques is subdivided according to general coding strategy, briefly describing their respective operating principles and highlighting their potential applicability in real-time setups. Section 3 discusses the associated problem of phase unwrapping. In Section 4, we give an overview of SLP systems that have been reported to operate in real-time and describe the main advances in digital projection technology and coding strategy that have led to their development. Section 5 discusses the strengths and weaknesses of single-shot versus multi-shot techniques in high-speed setups, summarizes the current limitations of state-of-the-art SLP techniques and describes future challenges. Finally, Section 6 concludes the paper.

2. Structured light profilometry techniques

The low-cost access to fast, high-resolution digital projection systems based on liquid crystal displays (LCD) and digital light projectors (DLP) has enabled the development of a wide variety of structured light profilometry techniques. Structured light or active illumination profilometry techniques illuminate the measurement object with predefined spatially varying intensity patterns and record these patterns as they are deformed by the object shape when observed at an angle with the projection axis. The basic setup of SLP techniques is illustrated in Fig. 1. A structured light modulator (*projector*) projects the pattern onto the scene and an imaging sensor (*camera*) placed at a relative angle with the projection axis records the deformed pattern. Digitalization of this basic projector–camera setup has enabled numerous SLP-techniques to be developed, each with their own respective strengths and weaknesses.

Though they are all unique in their specific implementation, differentiation between them can be made based on whether or not they require multiple projected patterns per 3D measurement (single-shot versus multi-shot techniques), whether or not they use color encoded projection schemes and specific coding strategy. A more precise schematic overview of the different classes of structured light projection techniques is presented in Fig. 2, analogous to the overview created by Geng [13]. Here, we have updated the overview with recently developed techniques, added the family of Fourier-based profilometry techniques and subdivided the set of phase shifting techniques according to their respective projected intensity profiles. Techniques which have been reported to reach real-time (> 10 3D frames per second) acquisition, digital signal processing and display of 3D surface maps are marked with an encircled 'R'-symbol. Techniques which require phase unwrapping (see Section 3) as part of their reconstruction algorithm are marked with an encircled 'PU'-symbol.

2.1. Color encoded projection techniques

Color encoded projection techniques employ color as a differentiating tool to uniquely label the object surface. The major advantage of color encoded projection techniques is their potential ability to acquire depth information using only a single projected image. Their disadvantage, however, lies in the fact that a color-independent reflectivity profile of the measurement target is assumed and that the quality of the resulting depth map is greatly influenced by the correspondence between projected and recorded color values. This makes them often unsuitable for practical applications that need to measure (partly) colored objects.

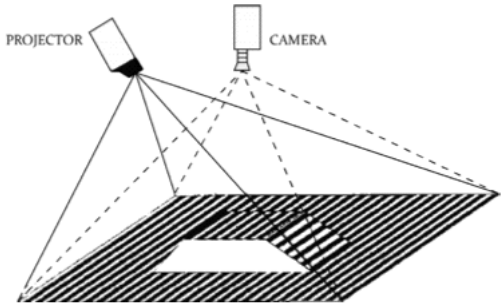

Fig. 1. Standard projector–camera configuration used in structured light profilometry techniques. Figure modified from Sansoni et al. [12].

Rainbow 3D cameras [14,15] illuminate the object with a spatially varying color pattern, establishing a one-to-one correspondence between the projection angle and a particular wavelength. This way, each surface point is landmarked with a specific wavelength and can be triangulated if the angle between the projection and camera axes is known. This technique is highly sensitive to the dynamic range and color resolution of the employed CCD chip: with a standard image sensor containing three 8-bit channels, a total of 2^{24} different colors can be represented. Correct triangulation implies a one-to-one correspondence between projected and recorded color value over this entire color range, making rainbow 3D cameras highly sensitive to cross-talk between color channels. By projecting *color coded stripes* [16] onto the target surface, the range of the color-sensitive CCD chip can be subdivided in discrete levels, reducing the in-plane resolution but making the technique more robust to color-dependent reflectivity profiles. A special color coded stripe sequence is based on the unique features of a *De Bruijn sequence* [17,18]. A De Bruijn sequence of rank n on a base set of size k is a cyclic word in which each of the k^n words of length n appears exactly once as we travel through the cycle. This way, a stripe pattern can be constructed that consists of uniquely identifiable local color patterns with a limited set of base colors. *Composite* color coding techniques superimpose multiple phase shifted patterns onto a single color image [19,20]. This color pattern is then projected onto the target statically and is recorded by a color-sensitive CCD chip. By separating the color channels in post-processing, the deformed phase shifted patterns can be reconstructed and the object height profile can be extracted using well-known phase shifting techniques. A combination of color coded stripes and composite color coding techniques consists of encoding multiple patterns into a single color projection image. This way, the ambiguity problem caused by employing phase shifted patterns can be alleviated [21,22]. In any case, one should reduce the decoding error rate by optimizing the color sets by maximizing the distance between adjacent colors in the projected pattern. Another type of color encoding strategy is to project both horizontal and vertical stripes onto the target so that a *color coded grid* is achieved. Adding this extra dimension of encoding facilitates solving the correspondence problem [23,24], although the limited thickness of the projected lines reduces the stability of this technique when compared to the above color encoded methods. Similarly, a *color coded dot array* of pseudo-randomized colored

Please cite this article as: Van der Jeught S, Dirckx JJJ. Real-time structured light profilometry: a review. Opt Laser Eng (2016), http://dx.doi.org/10.1016/j.optlaseng.2016.01.011

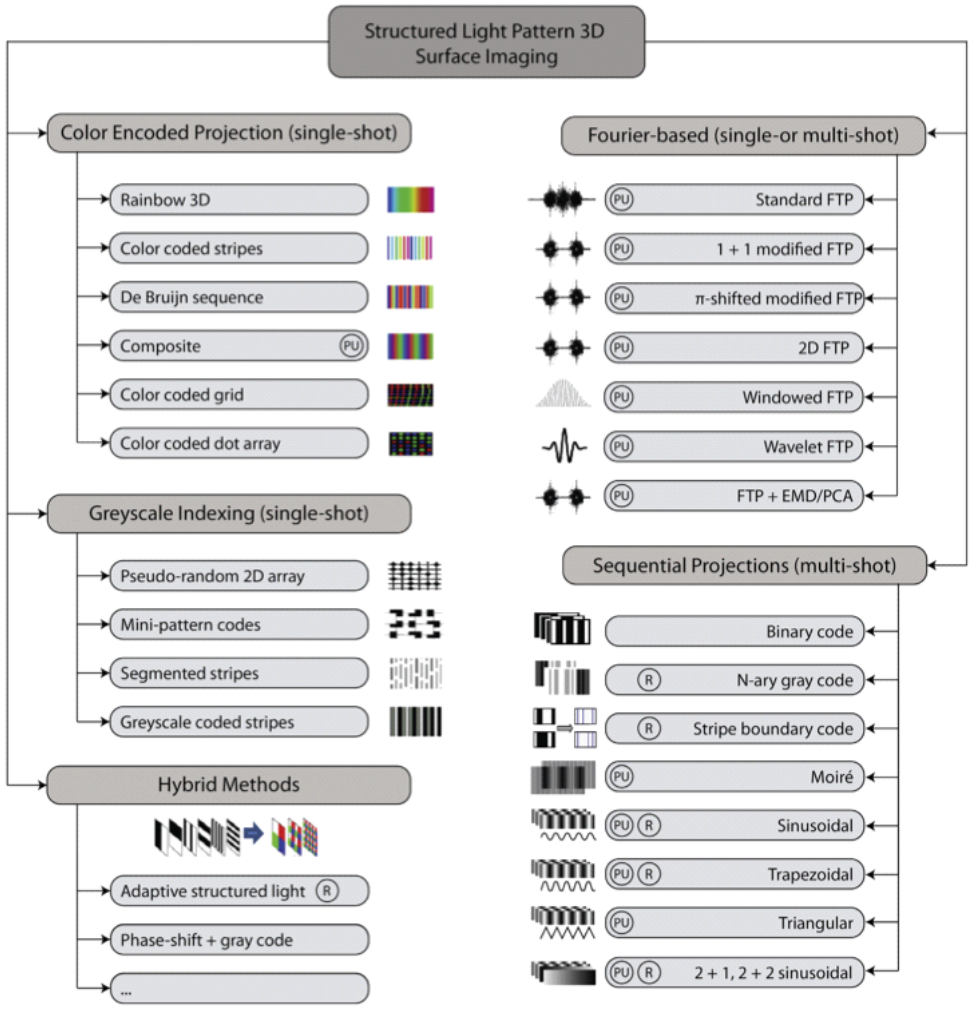

Fig. 2. Schematic overview of structured light profilometry techniques. Techniques that require phase unwrapping are marked with an encircled 'PU'-symbol, techniques that have been implemented in real-time are marked with an encircled 'R'-symbol.

If line is too deformed, can't match

pixels can be used to encode the object surface with a 2D color pattern. Brute force algorithms [25,26] have been used to ensure the uniqueness of subwindows of predefined size, though it has been reported that not all possible subwindow patterns may be exhausted [13].

2.2. Grayscale indexing

Grayscale indexing methods are single-shot techniques that project a series of dots, stripes or coded patterns onto the target and employ pattern search algorithms to solve the correspondence problem and to reconstruct the 3D object shape. They are color-independent methods which can be used to measure objects that contain non-uniform surface color distributions. On the other hand, as these techniques typically rely on recovering the deformed projected pattern within at least a subwindow of the projected pattern, they are sensitive to object surface discontinuities and require high in-plane resolving power.

One indexing strategy is to label the object surface with a *pseudo-random binary array* (PRBA) that contains binary dots on some of the intersections of a Cartesian grid [25,27]. By constructing the PRBA so that every subwindow of the projected pattern is unique, every coordinate location can be uniquely determined. Deformation of the 2D Cartesian dot pattern can then be used to triangulate the object depth at every intersection of the projected grid. Alternatively, *mini-patterns* can be used as code words to form a grid-indexed projection pattern [28] by arranging a set of mini-patterns in a pseudo-random 2D array so that every

Please cite this article as: Van der Jeught S, Dirckx JJJ. Real-time structured light profilometry: a review. Opt Laser Eng (2016), http://dx.doi.org/10.1016/j.optlaseng.2016.01.011

subwindow is unique. In analogy with the projection of color coded stripes, binary stripes can labeled by adding cuts at different predefined positions, dividing them in uniquely identifiable segment series [29]. This technique is commonly referred to as *segmented stripes* profilometry. Finally, *grayscale coded stripes* can be repeated in a pattern if more than two intensity levels are used. By arranging them such that any group of stripes within a certain period of length is unique, a pattern matching algorithm can be used to locate the individual deformed stripes [30].

2.3. Fourier-based profilometry

Another subset of grayscale SLP techniques that require only a single frame to retrieve the 3D object surface profile is the group of Fourier transform profilometry (FTP) techniques. In contrast to the grayscale indexing methods that project uniquely identifiable patterns onto the object, FTP techniques typically employ standard sinusoidal or *Ronchi* gratings to cover the entire object surface. This makes them less sensitive to image defocus when compared to indexing methods. On the other hand, as successful 3D reconstruction is determined by the correct selection of only the originally projected or *fundamental* frequency band in Fourier space, FTP techniques are nevertheless limited to a finite maximum slope of depth variation. Beyond this maximum, the fundamental frequency band overlaps the zero component and other high frequency components and cannot be retrieved unambiguously [31,32].

Originally, *standard FTP* was introduced by Takeda et al. [33] in 1982. Sinusoidal gratings are projected onto the object and appear deformed by the object surface shape when observed at an angle with the projection axis. Next, the obtained image is Fourier transformed row-per-row in the direction perpendicular to the projected patterns and the frequency spectrum is filtered to properly isolate the fundamental frequency which is broadened to a frequency band by the non-uniform slope distribution of the object surface shape. Inverse Fourier transform of only this frequency band results in a principle phase value ranging from $-\pi$ to π. After phase unwrapping (see below) and calibration, these phase values can be linked to the actual object depth.

In order to decrease overlapping with frequencies caused by features such as shadows, non-uniformities or contours that are present on the object surface itself, *1+1 modified FTP* techniques [34] record an additional image of the measurement target before projecting the Ronchi gratings. By subtracting this background image from the image containing the projected lines, only the deformed lines remain and the fundamental frequency band can be selected more easily from the obtained spectra. While this procedure significantly increases the measurement precision of the FTP technique, it does not completely remove frequency overlapping and requires an additional reference image of the uniformly lit target. Similarly, *π-shifted modified FTP* techniques [35] record an additional frame of the measurement target after the projected gratings are shifted over half a period. This way, the fundamental spectrum modulated by the object height distribution can theoretically be extended from 0 to $2\nu_0$, where ν_0 is the fundamental carrier frequency, without overlapping the zero- or higher frequency components. When measuring coarse objects with surface discontinuities or speckle-like structures, local loss of contrast around the projected fringes can hinder the row-per-row reconstruction of object phase. In order to accomplish automatic depth measurement of such objects, one might employ *two-dimensional (2D) FTP* techniques [36]. These techniques perform a two-dimensional Fourier transform of the entire observed fringe pattern, filter the resulting spectrum by a 2D Hanning window and perform an inverse Fourier transform to retrieve the object phase. It was demonstrated that 2D FTP techniques provide better separation of the fundamental frequencies from noise and diminishes the effect of local surface discontinuities on the resulting 3D depth measurement [37]. Alternatively, *windowed FTP* techniques [38–40] divide the entire fringe pattern into a limited set of local fringe regions by using a moving window. Next, each segment is Fourier transformed and all local spectra are superimposed to retrieve the entire fringe pattern's spectrum. By optimizing the window function and the projected fringe period to the specific measurement object surface, the effect of fringe noise can be suppressed and spectral leakage caused by local discontinuities in the fringe pattern can be reduced. Obviously, the computational cost of windowed FTP is significantly greater than that of standard FTP techniques. *Wavelet transform profilometry* techniques [41,42] also separate the signal in segments, but change the window function according to the local frequency. Typically, 1D *Paul* or *Morlet* mother wavelets are used [43] but 2D continuous wavelets have been reported as well [44,45]. In comparison to the Fourier transform, wavelet transforms are computationally more expensive, but can better detect the local characteristics of the fringe pattern which results in better measurement precision [40]. *Shearlets*, the natural extension of wavelets that were designed to better accommodate anisotropic features such as edges or borders in images, have recently been introduced in single-shot structured light profilometry [46]. It has been demonstrated that their superior directional sensitivity allows for better distinction between noise and fringes and improved general background removal [47]. Finally, *empirical mode decomposition (EMD)* [48,49] or *principle component analysis (PCA)* [50] techniques were introduced in FTP to extract the fundamental frequency band and to remove the non-linear carrier frequency caused by divergent illumination without the need for capturing multiple fringe patterns. With these methods, the recorded fringe patterns are adaptively decomposed into a finite number of intrinsic mode functions or principle components by using algorithms that are commonly referred to as sifting processes. This way, high frequencies can be separated from low frequencies and the zero-spectrum can be extracted more precisely [32].

2.4. Sequential projection techniques

Although the above methods have the distinct advantage of being single-shot techniques, their technical feasibility is often complicated by the specific reflective properties of the measurement target. Many objects cannot guarantee color-independent reflectivity profiles and limit the applicability of color encoded techniques. Similarly, a poorly reflecting surface layer drastically limits the resolution of methods which rely on the exact reconstruction of coded mini-patterns, binary dots or stripes from the acquired image. Finally, the measurement precision of FTP techniques suffers when the measurement object has a non-uniform or non-diffusely reflecting surface structure.

Consequently, speed may be sacrificed in favor of resolution and stability by using multi-shot techniques. Multi-shot or sequential projection techniques acquire multiple images of the object per 3D-measurement in a sequence of varying projected patterns.

The most straightforward multi-shot approach is to provide each point on the object surface with a unique *binary code* by illuminating it with a sequence of black and white horizontal and vertical stripes and extracting the depth information by matching the binary code words between the original and the deformed sequence [51]. Optimally, N binary patterns can generate $2N$ different code words per image dimension. This means that the binary coding technique requires a minimum of $2log_2(512)=18$ different projected patterns to uniquely describe a grid of 512×512 pixels. By dividing the projected intensities in M

Please cite this article as: Van der Jeught S, Dirckx JJJ. Real-time structured light profilometry: a review. Opt Laser Eng (2016), http://dx.doi.org/10.1016/j.optlaseng.2016.01.011

grayscale levels, N grayscale patterns can generate MN different code words per image direction. This way, *gray code* profilometry [52] can effectively increase the measurement speed of the profilometry technique by reducing the minimum amount of required patterns per image dimension. Binary code and gray code profilometry are generally robust techniques with relatively high tolerance for measurement noise since only discretized intensity regions are used in all pixels. On the other hand, the large amount of required frames per measurement significantly limits the acquisition speed. Furthermore, the height map produced by both binary and gray code profilometry techniques is determined by the successful detection of the smallest projected elements. Therefore, axial resolution and transversal resolving power of the imaging sensor are inherently coupled. Similar to binary code profilometry, *stripe boundary code* techniques [53,54] project a set of black and white illumination patterns onto the measurement target. Unlike binary (and gray) code techniques, however, stripe boundary code profilometry is based on time-codification of the boundaries between projected stripes. As these boundaries are tracked between subsequent frames, depth extraction is permitted even in the presence of moving objects in the scene. The incorporation of temporal coherence between subsequent frames within a single measurement cycle enables inter-frame tracking of object movement and limits motion artifacts in the reconstruction of the 3D surface shape model.

In order to increase axial resolution whilst limiting the required number of frames per 3D-measurement, phase shifting profilometry techniques [55–57] employ the entire dynamic range of the projector–camera system. In phase shifting profilometry, a sequence of fringe patterns with spatially varying intensity profiles and relative phase shifts between them are projected onto the object. The phase shifts caused by the non-planar object surface are extracted from the acquired deformed fringe patterns by calculating the relative intensity values pixel-per-pixel. Because they are *intensity ratio*-based techniques, phase shifting profilometry methods are generally well-suited to measure objects with poor overall or local reflective properties. The periodic nature of the technique, however, introduces the problem of ambiguous phase extraction and requires additional phase unwrapping calculations to retrieve the continuous phase map. This process is discussed below in Section 3.

Originally, phase shifting profilometry techniques employed a second demodulation grid which was placed between object and camera. When two (or more) slightly misaligned periodic arrays are superimposed onto the camera chip, their respective spatial frequency differences form a beat pattern commonly referred to as a *Moiré* pattern. If the projection and demodulation grid contain gratings with spatial pitches P_p and P_d, respectively, the pitch of the resulting Moiré interference fringes is increased to $P_pP_d/|P_p-P_d|$. This way, the camera does not need to resolve the projected grid lines individually and a relatively low-resolution camera can be employed. The earlier *shadow Moiré*-techniques [10,58] extracted height information from the interference pattern between the projection grid and its shadow on the object surface. Phase shifting was then performed by mechanically translating the object in the z-direction, causing the shadow lines to shift laterally. Alternatively, a second (different) grid was used between object and camera to demodulate the projected fringe pattern [59,60]. Relative phase-stepping was then achieved by laterally translating the projection and/or demodulation grid. Later, *projection Moiré*-techniques employed digital light projectors to directly project phase-shifted light patterns onto the object surface [61]. The deformed light patterns are then demodulated by a grating which is placed in front of the camera. Relative phase shifts between successive grating projections can now be controlled in software using the digital light projector. More recently, LCD grids have been used as both modulating and demodulating gratings [62–64] and the two-dimensional array of camera pixels itself has been used as a sub-or super-sampled demodulation grid [65].

With the increased availability of high-resolution, high dynamic range CCD-cameras, recent techniques have been developed that lack the second demodulation grid, but rather extract object depth information through direct analysis of the deformed grid patterns. Traditionally, these grid patterns have *sinusoidal* intensity profiles and the phase is recovered through calculation of an arctangent function. In order to replace the computationally time-consuming arctangent function with a straightforward intensity ratio calculation, Zhang et al. proposed a new three-step phase shifting algorithm which employed grids with *trapezoidal* intensity profiles [56,66]. As these patterns defocus and converge toward sinusoids over large object depths, the resulting phase errors are compensated by use of a lookup table. Both sinusoidal and trapezoidal phase shifting techniques require three or more images to correctly extract phase information. In contrast, *triangular* phase-shifting algorithms are able to reconstruct the object height using only two linear-coded triangular intensity patterns [67]. However, as triangular patterns are characterized by sharp corners, their measurement precision is more sensitive to projector gamma non-linearity and image defocus when compared to sinusoidal phase shifting techniques [68].

Finally, several sinusoidal phase shifting profilometry techniques have been reported that replace one or two of the phase-shifted fringe patterns of a 3-or 4-step projection cycle with a uniformly lit [69,70] or linearly increasing [71] intensity image or employ different fringe pattern frequencies in each of the projected images [72]. The 2+1 *modified sinusoidal* profilometry technique [69,70] requires two sinusoidal fringe pattern projections with a relative phase shift of $\pi/2$ and a third uniformly lit flat image of the measurement target to extract full-field depth information. This specific modification makes the 2+1 technique more suitable to measure moving targets, as the third, flat image is less sensitive to object motion between successive frames. On the other hand, the decrease in deformed fringe patterns from 3 to 2 per measurement cycle has a (slight) negative effect on the acquired measurement precision [73]. In addition, the three obtained images are no longer interchangeable and the order in which the 2+1 fringe patterns enter the digital signal processing pipeline becomes relevant. This requires additional signal processing to detect the uniformly lit image in the sequence or custom timing synchronization between projector and camera. Alternatively, the 2+2 *modified sinusoidal* profilometry technique [71] replaces the uniformly lit image of the measurement target with two linearly increasing/decreasing intensity ramp patterns to reconstruct the object surface profile. Although the requirement for an additional frame reduces the maximum obtainable 3D frame rate, it permits the calculation of a *base phase* which facilitates the phase unwrapping process and thereby significantly reduces the complexity of the reconstruction algorithm. Finally, phase error reduction has been demonstrated in 3-step phase shifting profilometry when the fringe pattern frequencies of successively projected images are chosen so that they obey certain general rules that confine their relative sizes to specific base frequency ratios [72].

2.5. Hybrid methods

When measurement speed is not an issue, an object surface can be mapped by any successive combination of structured light profilometry techniques in a single measurement. By selecting complementary techniques, the respective strengths of different methods can be cumulated and a higher quality 3D surface profile can be obtained. One of the most common combinations found in

Please cite this article as: Van der Jeught S, Dirckx JJJ. Real-time structured light profilometry: a review. Opt Laser Eng (2016), http://dx.doi.org/10.1016/j.optlaseng.2016.01.011

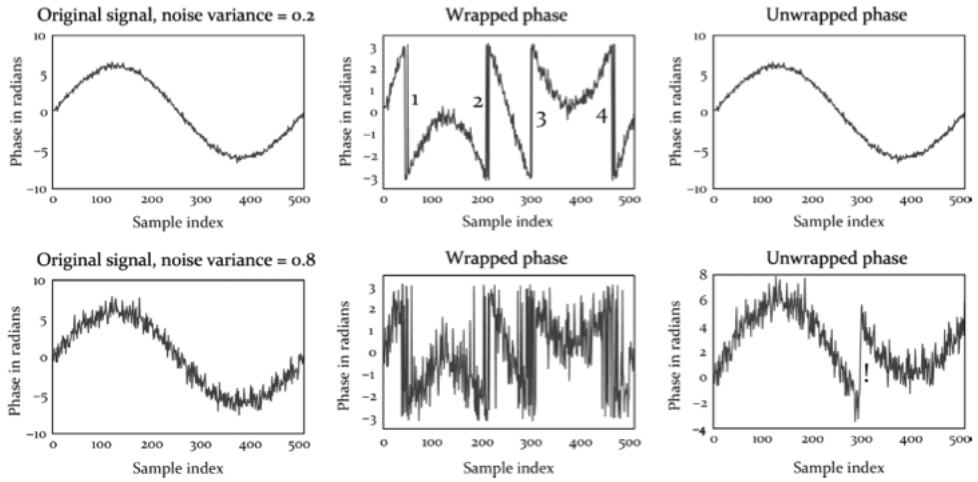

Fig. 3. Graphical representation of the one-dimensional phase unwrapping process. Top row: sine wave with added Gaussian noise (variance set to 0.2). Bottom row: sine wave with added Gaussian noise (variance set to 0.8). Four phase jumps (denoted by the numerators 1–4) are present in the wrapped signal. Rising noise levels cause the phase unwrapping procedure to miss one of the four phase jumps in the wrapped phase signal, leading to a distortion artifact (denoted by the exclamation mark) that propagates throughout the remainder of the signal.

Phase unwrap = convert from sine wave's range $[-\pi, \pi]$ to continuous

industrial applications that employ structured light to map the surface of static objects is the pairing of phase shifting techniques with binary or gray code profilometry [74,75]. The robustness against measurement noise of binary techniques allows for a first, rudimental surface map of the object to be formed of which the axial resolution can subsequently be improved using a set of phase shifting techniques. This way, the phase unwrapping procedure can be avoided and the 3D measurement becomes fully automated. Another way of avoiding the time-consuming and error-prone process of phase unwrapping is by combining multiple sets of phase shifting cycles in a dual- or multi-frequency pattern scheme. This can be achieved by either including one or more additional cycles with large fringe pitches so that the entire measurement falls within a single fringe plane [76], or by combining two or more sets of different fringe periods in the creation of a virtual fringe pattern with a larger equivalent pitch [77,78]. In addition, when the frequency ratio in multi-frequency pattern schemes is selected properly, non-linear phase errors generated by the inevitable non-sinusoidality of discretely sampled fringe patterns can be reduced [79]. Alternatively, composite fringe patterns have been constructed that contain both low- and high-frequency components [80–82]. Subsequent Fourier analysis of the obtained multi-frequency fringe patterns allows the reconstruction of the individual phase maps corresponding to each input frequency, the calculation of a unit-frequency phase map and the creation of phase partitions. Finally, Koninckx et al. [83–85] and Griesser et al. [86] have reported an *adaptive structured light* technique which optimizes the nature, color and/or amount of projected patterns in function of the object surface and measurement conditions. Depending on the object, sparse color coding of the base stripe pattern, superimposition of unique code points onto projected stripes or a combination is employed. Using a feedback loop, the projected patterns can be self-adapting to render the technique more robust against scene variability.

3. Phase unwrapping

Many of the structured light profilometry techniques obtain phase information that is mathematically constrained or 'wrapped' to its principal value domain. Typically, this constriction occurs when the digital signal processing technique used in the reconstruction algorithm employs an inverse- or arctangent function to retrieve the phase signal. Considering the principal value domain of the (four-quadrant) arctangent function, such phase signals are generally wrapped to the finite interval $[-\pi, \pi]$ and require custom digital signal processing techniques to remove the artificial 2π-discontinuities or 'phase jumps' from the signal. The procedure of extracting the original continuous phase from the wrapped input phase signal is commonly referred to as 'phase unwrapping'. It should be noted, though, that calculation of an arctangent function as part of the phase extraction algorithm is not an exclusive demand to require phase unwrapping. Structured light profilometry techniques which combine periodic fringe patterns with intensity ratio calculations generally also produce wrapped phase data, which can now be restricted to any finite interval, based on the projected intensity profiles and the employed reconstruction process. Nevertheless, whether the value of the phase jumps is 2π or any discrete number, the requirement for phase unwrapping stands and its basic principles remain valid.

In one-dimensional signals, the phase unwrapping problem is reduced to the detection and subsequent removal of phase jumps by adding an integer multiple of 2π to each sample value so that the numerical difference between neighboring sampling points is everywhere less than π. In practice, one starts from the second sampling point from the left in the wrapped phase signal and calculates the difference between the current sample and the one directly adjacent to the left. If this difference is larger than π, subtract 2π from the current sample and from all samples to the right of it. If the difference is smaller than $-\pi$, add 2π to the current sample and to all samples to the right of it. Move on to the third sample from the left and repeat this process until the last sample in the signal is reached. A graphical representation of the

Please cite this article as: Van der Jeught S, Dirckx JJJ. Real-time structured light profilometry: a review. Opt Laser Eng (2016), http://dx.doi.org/10.1016/j.optlaseng.2016.01.011

Table 1
Chronological overview of publications that have reported real-time acquisition, processing and displaying of 3D surface maps.

Author	SLP technique	Year of publication	Projection technique	CCD (pixels)	3D frame rate (fps)
Hall-Holt et al. [53], Rusinkiewicz et al. [54]	Stripe boundary code	2001, 2002	DLP	640x240	15
Huang et al. [107]	3-step sinusoidal	2003	DLP	640x480	16
Koninckx et al. [83–85], Griesser et al. [86]	Adaptive structured light	2003, 2004, 2006	LCD	640x480	10–25*
Zhang et al. [66,108]	3-step trapezoidal	2004, 2006	DLP	532x500	40
Pan et al. [109]	N-ary gray code	2004	DLP	640x480	40
Zhang et al. [64,100]	2+1 sinusoidal	2006, 2007	DLP	640x480	60
Liu et al. [111]	5-step dual frequency sinusoidal	2010	DLP-evaluation module	640x480	20
Zuo et al. [71]	2+2 sinusoidal	2012	DLP	640x480	30
Karpinsky et al. [78]	6-step dual frequency 3-step sinusoidal	2014	DLP-evaluation module	800x600	30
Van der Jeught et al. [112]	4-step sinusoidal	2015	DLP-evaluation module	640x480	30
Nguyen et al. [113]	3-step sinusoidal	2015	DLP	640x480	45

* Exact frame rate depends on scene complexity

one-dimensional phase unwrapping procedure is presented in Fig. 3.

A sine wave of amplitude larger than π is simulated, the signal is distorted with additive Gaussian noise and wrapped to the finite interval $[-\pi, \pi]$ by calculating its four-quadrant arctangent function. When noise levels remain sufficiently low, the phase unwrapping algorithm is able to detect the four phase jumps that are present in the wrapped phase and correct for them accordingly. However, when the signal suffers from higher noise levels or insufficiently dense signal sampling, it can have catastrophic effects on the outcome of the phase unwrapping procedure. This is illustrated in the bottom row of Fig. 3 where increased noise levels have caused the phase unwrapping algorithm to miss one of the four original phase jumps. Random noise has reduced the difference between the sampling points on either side of the third discontinuity to less than π and no phase jump is detected. Conversely, in addition to the miss of genuine phase jumps, higher noise levels or undersampling of the phase signal may also lead to the incorrect detection of 'fake' phase jumps, when the difference between adjacent continuous sampling points has been erroneously increased to more than π. As the phase unwrapping process is accumulative in nature, the resulting errors propagate throughout the remainder of the signal. This principle makes the design of robust phase unwrapping algorithms so challenging.

In two-dimensional signals, the phase unwrapping problem becomes vastly more complex and much more interesting. As phase jumps can occur both horizontally and vertically within the phase map, each pixel (barred those at the borders) now has four nearest neighbors that require discontinuity checking. In addition, the order in which pixels are unwrapped greatly determines the final outcome of the algorithm. Since expansion of the phase unwrapping algorithm to two dimensions does not void its accumulative nature, it is of crucial importance to avoid unwrapping artifacts early on in the phase unwrapping procedure. To this end, the classical approach to aid the two-dimensional phase unwrapping algorithm in selecting its optimal path of integration is to provide it with a pre-calculated pixel quality map. This way, high-quality pixels (or pixels with little local noise) can be unwrapped first and low-quality pixels (or pixels with high local noise) can be unwrapped last, limiting the propagation of errors throughout the unwrapped phase map. These processing schemes are commonly referred to as 'quality guided' phase unwrapping algorithms [87–89]. As a specific order of unwrapping is maintained and no two unwrapping operations can take place at the same time, this particular approach to phase unwrapping is inherently serial. In order to introduce some parallelism into two-dimensional phase unwrapping and to increase its potential processing speed, a host of phase unwrapping algorithms has been designed over the years that mainly provide varying compromises between the classic trade-off between speed and accuracy. Examples of theoretical principles that have been used to solve the two-dimensional phase unwrapping problem include the following: multi-level or discrete quality maps [90,91], Bayesian approaches [92], Markov random fields [93], region growing algorithms [94], neural networks [95], genetic algorithms [96], Green's functions [97], fractals [98], network flow algorithms [99], cellular automata [100], L_p-norm minimization [101] and statistical approaches [102]. Detailed descriptions of these methods fall outside the scope of the presented work, but it can be noted that what they all have in common is that the overall quality of phase unwrapping generally improves with increased processing time. Note also that the phase unwrapping problem can be expanded to 3 or even N dimensions. Although multi-dimensional expansion increases the complexity of the problem, many of the core principles upon which two-dimensional phase unwrapping algorithms are based can be transferred to solve the problem in N dimensions [103,104].

As phase unwrapping is a crucial step in many structured light profilometry techniques, their integration in digital processing pipelines is a common bottleneck in real-time applications that require phase data to be unwrapped before visualization. At the time of writing, only two reports have been made of phase unwrapping techniques that are able to operate in real-time set-ups. Zhang et al. [91] presented a multi-level approach with an optimized scan-line algorithm to process VGA resolution phase maps within 18.3 ms. Recently, we transferred the phase unwrapping problem to Fourier space and demonstrated <5 ms processing capability for VGA resolution phase data by using a graphics processing unit [105].

4. Real-time structured light profilometry

Though many structured light profilometry techniques have found their way into practical applications, only few of them are implemented in *real-time* setups. Table 1 provides a chronological overview of systems that have reported simultaneous acquisition, digital signal processing and display of full-field 3D surface maps in a continuous loop of at least 10 frames per second (fps). Although the threshold of 10 fps as qualification limit for a system to be 'real-time' is chosen somewhat arbitrarily, it does correspond to the speed limit at which the human visual system is found to be able to process and perceive different images individually [106]. Furthermore, it should be noted that we have normalized the reported 3D frame rates of the various sequential projection techniques by reducing their respective frame rate in case identical fringe patterns are re-used in subsequent processing cycles. This allows for a more objective comparison of the so-called pseudo-real-time systems with systems that employ only newly acquired fringe patterns every 3D measurement. In the remainder of the

Please cite this article as: Van der Jeught S, Dirckx JJJ. Real-time structured light profilometry: a review. Opt Laser Eng (2016), http://dx.doi.org/10.1016/j.optlaseng.2016.01.011

section, we describe the main advances in digital projection technology and coding strategy that have led to the development of these real-time structured light profilometry systems.

4.1. Digital fringe pattern projection

As previously stated, the advent of low-cost digital projection hardware has been instrumental to the development of real-time structured light profilometry techniques. One of the first systems to employ a digital video projector as a means to quickly shift between successive fringe pattern images in a multi-shot profilometry technique was presented by Hall-Holt et al. [53] and Rusinkiewicz et al. [54]. By projecting a four-frame sequence of binary fringe patterns onto the measurement target at a rate of 60 Hz, a unique surface map could be extracted from the deformed fringe patterns 15 times per second. By tracking the boundaries between black and white fringes between successive fringe projections, the system was able to correct for slow in-plane object motion (of between one-fourth and one-half stripe-width per frame) within a single measurement cycle. Whereas previous implementations of the *stripe boundary code*-based pipeline required human intervention at various stages of the 3D measurement process [114,115], digitalization and synchronization of the projector–camera system increased the level of automation, permitted the user to rotate the measurement target by hand and see a continuously-updated model as the object was scanned. This both increased user interaction and allowed for the construction of complete 3D surface models of the measurement target to be reconstructed at reasonably high speeds.

Similarly, the real-time adaptive structured light systems presented by Koninckx et al. [83–85] and Griesser et al. [86] employed fast digital projection hardware to modify the projected fringe patterns on-line. In contrast to other structured light profilometry techniques which employ static code patterns that are supposed to work under all circumstances, the digital signal processing speed of adaptive light techniques is dependent on the object properties and can therefore lead to varying 3D frame rates. By adapting the fringe pattern pitch, code line position and color markers in function of the texture and reflective properties of the object surface, measurement precision and system robustness could be increased. This online feedback-loop was controlled in system memory and was maintained in real-time by utilizing the high data transfer rate between the graphics card and the digital projector.

4.2. DLP modifications and digital micromirror devices

Ultimately, the speed of sequential or adaptive structured light profilometry techniques is limited by the transfer rate between graphics card and projector. At the time of writing, the maximum speed at which consumer-grade digital projection systems can switch between unique input frames is limited to 60 frames per second [73]. This means that if a digital projector cycles through sets of 3-or 4-step fringe patterns in a continuous loop, the maximum obtainable 3D frame rate of the corresponding profilometry system is limited to 20 fps or 15 fps, respectively. To this end, Huang et al. [107] modified a DLP to project three phase-shifted, sinusoidal fringe patterns at a switching speed of 300 Hz. DLP's typically contain a 2D array of digital micromirror devices (DMD's) which rotate over an angle at high speeds to reflect light either towards or away from the objective lens. This way, the intensity of every pixel in the formed image can be controlled individually. The red, green and blue (and sometimes cyan, magenta, yellow and/or white) color components of an image are separated by the DLP on-chip and are projected successively at high speeds by synchronizing the digital micromirror state with the position of a rapidly rotating color wheel. The high switching speed allows the projected color sequence to be interpreted by the human brain as a single full-color image. Huang et al. combined three phase-shifted sinusoidal fringe patterns into a single static RGB-color image that was projected by the DLP. By removing the color wheel of the projector and synchronizing the DLP-camera system, grayscale phase shifted images could be captured at a maximum speed of 300 Hz. The employed 85 fps camera was only able to capture a single phase-shifted fringe pattern every two projection cycles, however, resulting in an actual 3D measurement speed of 16 fps. Nevertheless, the principle of color separation in modified DLP's was demonstrated and the potential speed of multi-shot profilometry techniques was increased. Later, the same DLP-modification was used by Zhang et al. in a system with a 240 Hz DLP and a 262 fps camera [66,108]. Here, a full three-step pattern sequence was captured within two projection cycles, leading to a 3D measurement speed of 40 fps. Because the arctangent-function required in the digital signal processing pipeline to retrieve the phase map proved to be too time-consuming for real-time applications, a new intensity ratio technique was employed. Similar to trapezoidal phase shifting profilometry, the phase was determined from direct intensity ratio calculations of the captured intensity profiles. Instead of fringe patterns with trapezoidal intensity profiles, regular sinusoidal fringe patterns were projected and a look-up-table was constructed to correct for the systematic measurement errors in the intensity ratio map induced by the non-linearity of the fringe patterns. The entire digital signal processing pipeline, including a custom spatial phase unwrapping algorithm, was able to follow the camera's rate of acquisition and resulted in the reconstruction of 40 height maps per second.

Pan et al. employed the same setup as Huang and Zhang in a 3-step N-ary gray code system [109]. Here, the intensity values of all pixels in the 3 acquired images are digitized into N different levels (Pan implemented ternary $N=3$ and sextanary $N=6$ code patterns) and code words are determined along the decoding direction for each pixel at a rate of 40 fps. Since the authors define these code words periodically to increase lateral resolution, a process similar to phase unwrapping is required to extract the continuous phase map from the sawtooth-like phase profile. In general, N-ary gray code profilometry is more robust to random noise than phase shifting techniques that employ the same amount of fringe images, but has lower measurement accuracy since a smaller range of discretized intensity values are used to reconstruct the height map.

Later, Zhang et al. reduced motion errors by replacing the 3-step phase shifting profilometry technique with a 2+1 technique that requires two π-shifted fringe patterns and a uniformly lit image of the object [64,100]. After detection of the flat image, the three images are combined into a single 3D measurement. The main advantage of this technique is the fact that every third image of the projected cycle is now unimpeded by object motion, making it less sensitive to movement of the measurement target between successive frames. Additionally, inclusion of a flat image in the measurement cycle allows for direct texture acquisition of the object surface which is an important asset in applications such as face recognition, computer vision, computer graphics, etc. Meanwhile, a higher-speed 180 fps camera was used in the experimental setup and a 3D frame rate of 60 fps was obtained. Other reports of real-time setups that employ modified consumer-grade DLP's include implementations of 2+2 sinusoidal profilometry [71] and 3-step sinusoidal profilometry [113].

More recently, compact DMD discovery boards became available that contain a digital micromirror device with on-board flash memory for pattern storage (http://www.ti.com/tool/dlplightcrafter). Though the light source and the projection optics on these

Please cite this article as: Van der Jeught S, Dirckx JJJ. Real-time structured light profilometry: a review. Opt Laser Eng (2016), http://dx.doi.org/10.1016/j.optlaseng.2016.01.011

modules are basic, they provide access to the DMD controller board and allow the user to cycle through predefined 8-bit patterns at a rate of up to 120 Hz and through binary patterns at a rate of up to 4000 Hz. In addition, these evaluation modules provide configurable I/O triggers for synchronization with cameras, sensors, etc. Liu et al. were the first to implement a Texas Instruments Discovery 1100 board in their real-time setup as projection engine to a dual frequency projection scheme [111]. Moving hand gestures were scanned using 6 patterns per 3D measurement, yielding a 3D frame rate of 20 fps. Later, Karpinsky et al. increased this frame rate to 30 fps by synchronizing the binary projection mode of a Texas Instruments Lightcrafter board with a 180 Hz camera [78]. Recently, we used the Lightcrafter board to inject structured light patterns into one of two optical pathways of a surgical stereomicroscope. After synchronization with a high-speed camera that was placed in the second optical pathway, we were able to acquire, process and display 30 microscopic height maps per second using standard 4-step sinusoidal phase shifting profilometry. This allowed the qualitative depth perception of the stereomicroscope operator to be enhanced by live quantitative height measurements with depth resolutions in the micrometer range [112].

4.3. Dual frequency projection to avoid phase unwrapping

Robust spatial phase unwrapping algorithms are generally computationally intensive and their design typically requires multiple iterations to reach convergence, leading to high execution times. Very basic phase unwrapping techniques such as flood-fill and scan-line algorithms have been reported to work in real-time [108], but they are very sensitive to noise and often generate artifacts that significantly reduce the quality of the height map. The multi-level phase unwrapping algorithm designed by Zhang et al. [91] combines the speed of scan-line algorithms with the robustness of multi-level techniques. However, it still relies on entirely continuous and connected phase maps as input, making the profilometry system unsuitable for measurements of objects containing isolated regions or phase discontinuities greater than one period. To this end, multi-frequency techniques have been employed in real-time setups to avoid spatial phase unwrapping, at the cost of an increased number of fringe patterns per projection cycle. Liu et al. [111] proposed a 5-pattern dual-frequency pattern scheme that combines a high-frequency component with a low-frequency component into a single fringe pattern. The high-frequency component generates a high-resolution wrapped phase map while the low-frequency component provides a base phase map that can be used to guide the phase unwrapping procedure of the high-frequency map. Alternatively, Zuo et al. [71] propose a four-pattern algorithm containing two π-shifted fringe planes and two linearly increasing/decreasing intensity planes to construct the base phase map. Finally, Karpinsky et al. [78] adopt a two-frequency 6-step phase shifting algorithm with different fringe pitches. These fringe pitches P_1 and P_2 are combined into a virtual fringe pattern with an *equivalent* fringe pitch of $P_1P_2/|P_1-P_2|$. By properly selecting the spatial frequencies of the dual-frequency patterns, an equivalent phase map can be constructed that spans the entire image without 2π-discontinuities.

The major advantage of multi-frequency projection techniques is the fact that the problem of phase unwrapping is reduced to the calculation of an additional phase map, after which a simple pixel by pixel subtraction and rounding operator suffices to reconstruct the absolute phase map. Second, having a low-frequency base phase allows for the measurement of multiple, non-connected objects or allows the imaged object to contain isolated patches. Finally, all of these calculations can be done concurrently on all pixels, making the technique highly suitable for parallel implementation. Besides the obvious disadvantage of requiring additional images, multi-frequency techniques contain projection cycles of which the fringe patterns are no longer interchangeable. In contrast to regular 3-or 4-step phase shifting profilometry, the order in which the fringe patterns are recorded is relevant to the reconstruction algorithm. This requires either additional digital signal processing to detect the various projected patterns or custom triggering between DLP and camera to mark the beginning of each measurement cycle.

4.4. GPU's and parallel processing pipelines

As the frame rate of structured light profilometry techniques increases, the amount of processing power required to reconstruct and visualize the 3D surface profile increases as well. In the early days of real-time phase shifting profilometry, direct calculation of the arctangent function (e.g. atan2 in C++) proved to be too slow to extract the phase from sinusoidal fringe patterns in real-time applications. In order to avoid this computational bottleneck, Zhang et al. developed a whole new phase shifting profilometry technique involving trapezoidal intensity profiles and look-up-tables to approximate the arctangent function [66,108]. Meanwhile, processing hardware has evolved in such a way that arctangent calculations can be calculated efficiently at reasonably high speeds, allowing the direct extraction of phase maps in real-time systems [78,112]. An important factor in this evolution is the increase in processing power of multicore parallel hardware over the last decade and the development of general-purpose graphics processing unit (GPGPU) programming [116]. Graphics processing units are specialized co-processors to the central processing unit (CPU) that were initially designed to perform graphics rendering tasks. Because of their recent increase in processing power, modern GPU's are commonly adopted in high-performance computing setups in scientific, engineering, analytics and consumer applications. GPU's typically contain a large number of streaming processors that operate concurrently and therefore require a custom parallel programming approach. In general, phase shifting profilometry techniques are highly suitable for parallel implementation as the phase value at each pixel coordinate can be calculated independently from those at neighboring pixels.

Zhang et al. reported a 4 × increase in processing speed using a Quadro FX 3450 GPU over a dual 3.4 Ghz CPU workstation in their real-time 2+1 phase shifting profilometry system [69]. Karpinsky et al. employed a Quadro NVS5400M GPU in their dual-frequency system to enable phase wrapping, base phase unwrapping, Gaussian filtering, normal calculation and 3D rendering at a frame rate of 30 Hz [78]. Recently, we developed a real-time noise-resistant spatial phase unwrapping algorithm by transferring the periodic phase unwrapping problem to Fourier space and by optimizing it for implementation on parallel hardware [105]. We have demonstrated its real-time capabilities ($<$ 5 ms for a 640 × 480 pixel phase map) and robustness to image noise on phase maps that were gathered with regular 4-step sinusoidal phase shifting profilometry, both in real-time macroscopic [105] and microscopic [112] setups.

One of the major bottlenecks in GPGPU programming is caused by the limited bandwidth of the PCI bus across which data between host (CPU) memory and device (GPU) memory is transferred. In order to hide this latency, the real-time profilometry pipeline needs to be organized in such a way that its architecture enables maximum concurrency of acquisition, memory transfer, digital signal processing and visualization. In Fig. 4, we present a schematic overview of such a pipeline that is optimized for real-time 4-step phase shifting profilometry [112]. At all times, fringe pattern acquisition, digital signal processing and on-screen rendering of successive measurements are executed in parallel. Following the data processing cycle of one 3D measurement (blue,

Please cite this article as: Van der Jeught S, Dirckx JJJ. Real-time structured light profilometry: a review. Opt Laser Eng (2016), http://dx.doi.org/10.1016/j.optlaseng.2016.01.011

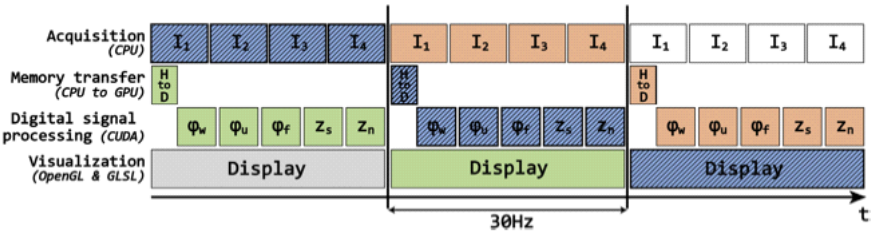

Fig. 4. Schematic overview of a real-time 4-step phase shifting profilometry pipeline. Horizontally aligned blocks occur sequentially; vertically aligned blocks occur simultaneously.

diagonally hatched), four input fringe patterns $I_1 - I_4$ are captured by the high-speed camera every 33.33 ms and are transferred from CPU to GPU memory. Next, the digital signal processing pipeline performs successive wrapped phase extraction (φ_W), phase unwrapping (φ_U), Gaussian filtering (φ_f), phase-to-height conversion and scaling (z_S) and normal calculation (Z_N). Finally, the height and normal maps are combined to render the 3D height measurement. It should be noted that the digital signal processing and memory transfer blocks as illustrated in Fig. 4 are not scaled to represent the respective time they take, but are in fact expanded to fill the maximum time slot they could take up without obstructing the real-time pipeline. In reality, the entire digital signal processing scheme, including memory transfer from host to device, takes up only 16.3 ms in total on a workstation containing a GTX770 graphics card and a dual core Intel i5 processor.

4.5. Binary defocus and ultra-fast 3D measurement speed

Although a 3D frame rate of 30–60 fps is sufficiently fast to capture slow object motion, higher speeds may be necessary if one wants to measure faster moving objects such as, for example, beating hearts, vibrating membranes or rotating fan blades. The most important feature of such ultrahigh-speed setups is not to process the acquired phase maps in real-time (the effect of adding more frames per second beyond 30 becomes negligible to human perception anyway) but to shorten the acquisition window so that the effect of motion artifacts may be reduced. In this regard, a sensible strategy would be to employ single-shot structured light profilometry techniques, since in that case a static fringe pattern may be projected and the 3D frame rate is limited only by the acquisition speed of the camera. Although pre-designed mechanical gratings or custom patterns may be used in combination with a continuous light source to illuminate the object with a static fringe pattern, they lack the flexibility of digital projection hardware.

To this end, Gong et al. reported the use of an off-the-shelf DLP projector in combination with standard Fourier transform profilometry to reach a 3D rate of 4000 Hz [117]. Instead of projecting a static 8-bit pattern onto the object, which would limit the pattern projection rate to the refresh rate of the DLP device, a static binary pattern (each pixel set to either 0 or 255) was used. Due to the fundamental image generation mechanism of DMD's, this resulted in the micromirrors being fixed in either the ON or OFF position 100% of the time. Since DLP's employ a continuous LED/Laser lamp light source, customizable binary digital fringe patterns can be projected in a static loop without glitches. Gong et al. realized that the binary nature of the produced fringe patterns was less than ideal for the application of Fourier transform profilometry, so they applied the *binary defocusing* technique proposed by Su et al. [118] and Lei et al. [119]. By deliberately defocusing the binary patterns, sinusoidal fringe patterns can be approximated at the cost of reduced contrast.

Alternatively, the binary projection mode of DLP evaluation modules allows projection of binary fringe patterns at display rates of 4000–10,000 Hz, depending on the controller board model and pixel resolution. Takei et al. [120], Zhang et al. [121], Wang et al. [77] and Zuo et al. [122] employed different models of the TI Discovery board in ultrahigh-speed profilometry systems based on various combinations of binary code and sinusoidal phase shifting profilometry. Sinusoidal fringe patterns were obtained through regular binary defocusing [121] or by modifying the binary patterns according to the *optimal pulse width modulation* technique [77,122]. This technique selectively eliminates undesired frequency components by inserting different types of notches into a conventional binary square wave in order to generate higher-quality sinusoidal fringe patterns. These systems enabled 3D acquisition rates in the order of hundreds to thousands of full-field height measurements, depending on the technique and the employed camera.

5. Discussion

5.1. Single-shot versus multi-shot techniques

Although single-shot structured light profilometry techniques have inherent speed advantages over multi-shot techniques, there are only a few reports of them being used in real-time systems [83–86]. The relative underrepresentation of single-shot techniques in real-time 3D surface measurement applications may be due to the fact that extensive digital signal processing is required to extract high-quality full-field height maps from a single frame. For example, if one wants to automate the otherwise manual procedure of fundamental frequency selection in Fourier transform profilometry, additional data operations such as window filtering or empirical mode decomposition are necessary. Even when implemented on parallel hardware, windowed FTP techniques have been reported to be limited to 4 frames per second for maps of 256×256 pixels [123]. Furthermore, the measurement accuracy of single-shot techniques is generally determined by the uniform, color-independent reflection profile of the measurement target surface [124]. To reduce the effect of cross-talk between different color channels and thereby to minimize its adverse effect on axial resolution, extra color decoupling calculations are required. Unfortunately, these algorithms are known to be very time-consuming [125,126]. In addition, most measurement targets in structured light profilometry applications contain non-uniform surface reflectivity profiles. Poor local reflection causes fringe pattern contrast to diminish and measurement accuracy to drop. In general, single-shot techniques are more sensitive to such contrast variations than multi-shot techniques since they are

Please cite this article as: Van der Jeught S, Dirckx JJJ. Real-time structured light profilometry: a review. Opt Laser Eng (2016), http://dx.doi.org/10.1016/j.optlaseng.2016.01.011

unable to assess the local reflectivity in function of the projected intensity level. Multi-shot techniques, on the other hand, do have the opportunity to account for non-uniform reflectivity profiles by incorporating intensity-ratio calculations in their height extraction algorithms. By dividing successive frames that have been illuminated with different intensity levels on a pixel-per-pixel basis, local reflectivity is normalized and measurement accuracy increased. This explains why the majority of reported real-time SLP techniques that have been used in practical applications are based on multi-shot intensity-ratio algorithms.

5.2. Challenges

It seems that the main challenges facing real-time surface measurement systems are threefold: first, fringe projection speed is currently the limiting factor in the frame rate of 3D structured light profilometry systems. In order to increase maximum potential imaging speed, projection hardware technologies need to improve. Second, structured light profilometry systems are rather large in size and weight and should be miniaturized to become implementable in practical medical or consumer-grade applications. Third, digital signal processing pipelines need to be able to keep up with the increasing rate of fringe plane acquisition. To this end, the design of parallel pipelines and the optimization of height extraction kernels to run on parallel hardware could become increasingly important.

Currently, the fastest 3D shape measurement systems [69,110] are able to produce 60 height maps per second, which is still not fast enough for many real-time applications. In order to measure fast-moving object surfaces such as beating hearts, rapidly speaking human face contours or rotating fans in real-time, imaging speeds of up to 300–400 3D frames/sec might be mandatory [73]. These speeds may be obtainable by using the binary defocusing technique in combination with DLP evaluation modules, but here axial resolution is sacrificed in favor of speed. If one wants to maintain true 8-bit grayscale projection of fringe patterns, DMD switching speed needs to increase. As there is no incentive for off-the-shelf projector manufacturers to increase DLP frame rate (as these are already above the maximum input signal refresh rate and the speed threshold for human sight already), advancements in this area are to be expected to come from DLP evaluation modules that are designed specifically for this purpose.

Projection hardware is also generally the largest component in real-time structured light profilometry systems. CCD-based cameras and lens optics are rather small and portable laptop computers have been shown to provide sufficient computational power to support real-time pipelines [78] but typical projection hardware is comparatively large and heavy. Conventionally, halogen lamps are used in commercial LCD or DLP projectors. These lamps generate a large amount of heat and require extensive cooling mechanisms. Recently, halogen lamps have been replaced with LED lamps in projection hardware developed by multiple companies including Mitsubishi, Samsung, Dell, Lg and Hitachi [73]. These lamps can be made much smaller and typically generate less heat, which has led to their incorporation into smaller DLP evaluation modules. Although these modules do allow more compact and portable 3D surface shape measurement systems to be assembled [78,112], the resulting projector-camera systems might need additional miniaturization to become practical in handheld 3D scanning applications. Furthermore, evaluation module light source power emission is still too low (typically several tens to several hundreds of lumen) to produce high-quality results in suboptimal lighting conditions.

Simultaneous acquisition, digital signal processing and displaying of surface maps in a triple-buffer strategy (Fig. 4) is a good way to distribute the workload across multiple co-processors as it enables thread concurrency and reduces system latency. Parallel processing pipelines ensure that height extraction and possible phase unwrapping kernels get allotted the maximum amount of processing time available. These time slots are ultimately limited by the total acquisition time of the full fringe plane acquisition cycle, which, depending on the required amount of fringe planes per measurement cycle, falls within the order of tens of milliseconds in high-speed systems. Therefore, real-time structured light profilometry systems require optimized kernel design and specialized parallel hardware such as graphics cards to follow the rate of acquisition. Although the clock speed and number of multiprocessors on graphics cards increases with each new generation, it has been demonstrated that the largest bottleneck in GPU-based applications is caused by the memory transfers between host and device memory [116]. As each new set of input fringe data needs to be moved from host to device, structured light profilometry techniques are heavily dependent on PCI-bus bandwidth. Currently, PCI-E bus bandwidth is limited to 5 GB/s at peak performance if optimal data transfer sizes are chosen and pinned memory is used. As real-time SLP systems require the transfer of many small data blocks, memory transfer speed can be up to an order of magnitude lower, on average [112]. Unless multiple fringe cycles are bundled in a single data transfer and a slight lag is allowed, a memory transfer penalty of several milliseconds per measurement is to be expected. Ideally, the PCI bus should be bypassed altogether by enabling the CCD camera to offload image buffers directly into GPU memory, but at the time of writing this feature is not supported by current hardware.

6. Conclusion

The last decade has witnessed a tremendous advance in the development of real-time structured light profilometry setups, both in terms of speed and of quality. Technological improvements in digital projection hardware and optimization of coding strategy have resulted in the production of several optical profilometry systems that are able to produce high-quality three-dimensional surface maps of dynamically moving targets at a refresh rate of several tens of frames per second. In this paper, we have presented the underlying principles that allow these surface mapping systems to operate in real-time and have discussed the remaining challenges that need to be tackled towards further improvement.

Acknowledgments

Sam Van der Jeught acknowledges the support of the Research Foundation - Flanders (FWO) (Grant no. 12/4916N).

References

[1] Ringbeck T, Hagebeuker B. A 3D time of flight camera for object detection. Opt. 3D. Meas Tech 2007:1–10. http://dx.doi.org/10.1038/sj.jcbfm.9600416.
[2] Lange R, Seitz P. Solid-state time-of-flight range camera. IEEE J Q Electron 2001;37:390–7. http://dx.doi.org/10.1109/3.910448.
[3] Hsu S, Acharya S, Rafii A, New R. Performance of a time-of-flight range camera for intelligent vehicle safety applications. Adv Microsyst Automot Appl 2006;2006:205–19. http://dx.doi.org/10.1007/3-540-33410-6_16.
[4] Zhang RZR, Tsai P-STP-S, Cryer JE, Shah M. Shape-from-shading: a survey. IEEE Trans Pattern Anal Mach Intell 1999:21. http://dx.doi.org/10.1109/34.784284.
[5] Brooks MJ, Horn BKP. Shape and source from shading. Shape Shading 1989:53–68.
[6] Nayar SK, Nakagawa Y. Shape from focus. IEEE Trans Pattern Anal Mach Intell 1994;16:824–31. http://dx.doi.org/10.1109/34.308479.

Please cite this article as: Van der Jeught S, Dirckx JJJ. Real-time structured light profilometry: a review. Opt Laser Eng (2016), http://dx.doi.org/10.1016/j.optlaseng.2016.01.011

[7] Torreão JRA, Fernandes JL. Single-image shape from defocus. Brazilian Symp. Comput Graph Image Process 2005;2005:241–6. http://dx.doi.org/10.1109/SIBGRAPI.2005.47.
[8] Brown MZ, Burschka D, Hager GD. Advances in computational stereo. IEEE Trans Pattern Anal Mach Intell 2003;25:993–1008. http://dx.doi.org/10.1109/TPAMI.2003.1217603.
[9] Scharstein D, Szeliski R. A taxonomy and evaluation of dense two-frame stereo correspondence algorithms. Int J Comput Vis 2002;47:7–42. http://dx.doi.org/10.1023/A:1014573219977.
[10] Meadows DM, Johnson WO, Allen JB. Generation of surface contours by moiré patterns. Appl Opt 1970;9:942–7. http://dx.doi.org/10.1364/AO.9.000942.
[11] Chiang C. Moiré topography. Appl Opt 1975;14:177–9. http://dx.doi.org/10.1364/AO.14.000177.
[12] Sansoni G, Biancardi L, Minoni U, Docchio F. Novel, adaptive system for 3-D optical profilometry using a liquid crystal light projector. IEEE Trans Instrum Meas 1994;43:558–66. http://dx.doi.org/10.1109/19.310169.
[13] Geng J. Structured-light 3D surface imaging: a tutorial. Adv Opt Photon 2011;3:128. http://dx.doi.org/10.1364/AOP.3.000128.
[14] Geng J. Rainbow three-dimensional camera: new concept of high-speed three-dimensional vision systems. Opt Eng 1996;35:376–83.
[1] Weinberg SM, Scott NM, Neiswanger K, Brandon CA, Marazita ML. Digital three-dimensional photogrammetry: evaluation of anthropometric precision and accuracy using a Genex 3D camera system. Cleft Palate-Craniofacial J 2004;41:507–18. http://dx.doi.org/10.1597/03-066.1.
[16] Liu W, Wang Z, Mu G, Fang Z. Color-coded projection grating method for shape measurement with a single exposure. Appl Opt 2000;39:3504–8.
[17] MacWilliams FJ, Sloane NJA. Pseudo-random sequences and arrays. Proc IEEE 1976;64:1715–29. http://dx.doi.org/10.1109/PROC.1976.10411.
[18] Zhang LZL, Curless B, Seitz SM. Rapid shape acquisition using color structured light and multi-pass dynamic programming, In: Proceedings First International Symposium on 3D Data Process Visual Transm, 2002, doi:10.1109/TDPVT.2002.1024035.
[19] Zhang Z, Towers CE, Towers DP. Time efficient color fringe projection system for 3D shape and color using optimum 3-frequency Selection. Opt Express 2006;14:6444–55. http://dx.doi.org/10.1364/OE.14.006444.
[20] Zhou C, Liu T, Si S, Xu J, Liu Y, Lei Z. An improved stair phase encoding method for absolute phase retrieval. Opt Lasers Eng 2015;66:269–78. http://dx.doi.org/10.1016/j.optlaseng.2014.09.011.
[21] Boyer KL, Kak AC. Color-encoded structured light for rapid active ranging. IEEE Trans Pattern Anal Mach Intell 1987;9:14–28. http://dx.doi.org/10.1109/TPAMI.1987.4767869.
[22] Fernandez S, Salvi J, Pribanic T. Absolute phase mapping for one-shot dense pattern projection, In: Proceedings of the 2010 IEEE Computer Society Conference on Computer Vision Pattern Recognition - Work. CVPRW 2010, 2010, pp. 64–71. doi:10.1109/CVPRW.2010.5543483.
[23] E.M. Petriu Z. Sakr H.J.W. Spoelder A. Moica Object recognition using pseudo-random color encoded structuredlight, In: Proceeedings of the 17th IEEE Instrumentation and Measurement Technology Conference, [Cat No 00CH37066] 2000, 3, doi: 10.1109/IMTC.2000.848675.
[24] Salvi J, Pagès J, Batlle J. Pattern codification strategies in structured light systems. Pattern Recognit 2004;37:827–49. http://dx.doi.org/10.1016/j.patcog.2003.10.002.
[25] P. Payeur D. Desjardins Structured light stereoscopic imaging with dynamic pseudo-random patterns. LNCSLect. Notes Comput. Sci. (including Subser. Lect. Notes Artif. Intell. Lect. Notes Bioinformatics) vol. 5627 2009 687 696 doi: 10.1007/978-3-642-02611-9_68.
[26] Desjardins D, Payeur P. Dense stereo range sensing with marching pseudo-random patterns. Proc. - Fourth Can. Conf. Comput. Robot Vision, CRV 2007, 2007, pp. 216–223. doi:10.1109/CRV.2007.22.
[27] Le Moigne JJ, Waxman AM. Structured light patterns for robot mobility. IEEE J Robot Autom 1988;4:541–8. http://dx.doi.org/10.1109/56.20439.
[28] Griffin PM, Narasimhan LS, Yee SR. Generation of uniquely encoded light patterns for range data acquisition. Pattern Recognit 1992;25:609–16. http://dx.doi.org/10.1016/0031-3203(92)90078-W.
[29] Maruyama M, Abe S. Range sensing by projecting multiple slits with random cuts. IEEE Trans Pattern Anal Mach Intell 1993;15:647–51. http://dx.doi.org/10.1109/34.216735.
[30] Durdle NG, Thayyoor J, Raso VJ. An improved structured light technique for surface reconstructionof the human trunk. Conf Proceedings IEEE Can Conf Electr Comput Eng (Cat No98TH8341) 1998;2. doi:10.1109/CCECE.1998.685637.
[31] Chen W, Su X, Cao Y, Zhang Q, Xiang L. Method for eliminating zero spectrum in Fourier transform profilometry. Opt Lasers Eng 2005;43:1267–76. http://dx.doi.org/10.1016/j.optlaseng.2004.12.002.
[32] Li S, Su X, Chen W, Xiang L. Eliminating the zero spectrum in Fourier transform profilometry using empirical mode decomposition. J Opt Soc Am A Opt Image Sci Vis 2009;26:1195–201. http://dx.doi.org/10.1364/JOSAA.26.001195.
[33] Takeda M, Mutoh K. Fourier transform profilometry for the automatic measurement of 3-D object shapes. Appl Opt 1983;22:3977. http://dx.doi.org/10.1364/AO.22.003977.
[34] Hong G, Huang P. 3-D shape measurement by use of a modified Fourier transform method. Proc SPIE 2008;7066:70660E.
[35] Li J, Su X- Y, Gou L- R. An improved Fourier transform profilometry for automatic measurement of 3-D object shapes. Opt Eng 1990;29:1439–44.
[36] Lin JF, Su X- Y. Two-dimensional Fourier transform profilometry for the automatic measurement of three-dimensional object shapes. Opt Eng 1995;34:3297–302.
[37] Su X, Chen W. Fourier transform profilometry: a review. Opt Lasers Eng 2001;35:263–84. http://dx.doi.org/10.1016/S0143-8166(01)00023-9.
[38] Berryman F, Pynsent P, Cubillo J. The effect of windowing in Fourier transform profilometry applied to noisy images. Opt Lasers Eng 2004;41:815–25. http://dx.doi.org/10.1016/S0143-8166(03)00061-7.
[39] Kemao Q. Windowed Fourier transform for fringe pattern analysis. Appl Opt 2004;43:2695–702. http://dx.doi.org/10.1364/AO.43.002695.
[40] Huang L, Kemao Q, Pan B, Asundi AK. Comparison of Fourier transform, windowed Fourier transform, and wavelet transform methods for phase extraction from a single fringe pattern in fringe projection profilometry. Opt Lasers Eng 2010;48:141–8. http://dx.doi.org/10.1016/j.optlaseng.2009.04.003.
[41] Zhong J, Weng J. Spatial carrier-fringe pattern analysis by means of wavelet transform: wavelet transform profilometry. Appl Opt 2004;43:4993–8. http://dx.doi.org/10.1364/AO.43.004993.
[42] Li H, Yang C. Two-dimensional multiscale windowed Fourier transform based on two-dimensional wavelet transform for fringe pattern demodulation. Opt Laser Technol 2011;43:72–81. http://dx.doi.org/10.1016/j.optlastec.2010.05.007.
[43] Gdeisat MA, Abid A, Burton DR, Lalor MJ, Lilley F, Moore C, et al. Spatial and temporal carrier fringe pattern demodulation using the one-dimensional continuous wavelet transform: recent progress, challenges and suggested developments. Opt Lasers Eng 2009;47:1348–61. http://dx.doi.org/10.1016/j.optlaseng.2009.07.009.
[44] Gdeisat MA, Burton DR, Lalor MJ. Spatial carrier fringe pattern demodulation by use of a two-dimensional continuous wavelet transform. Appl Opt 2006;45:8722–32. http://dx.doi.org/10.1364/AO.45.008722.
[45] Li S, Su X, Chen W. Spatial carrier fringe pattern phase demodulation by use of a two-dimensional real wavelet. Appl Opt 2009;48:6893–906. http://dx.doi.org/10.1364/AO.48.006893.
[46] Li B, Tang C, Zhu X, Su Y, Xu W. Shearlet transform for phase extraction in fringe projection profilometry with edges discontinuity. Opt Lasers Eng 2016;78:91–8. http://dx.doi.org/10.1016/j.optlaseng.2015.10.007.
[47] Lim WQ. The discrete shearlet transform: a new directional transform and compactly supported shearlet frames. IEEE Trans Image Process 2010;19:1166–80. http://dx.doi.org/10.1109/TIP.2010.2041410.
[48] Huang NE, Shen Z, Long SR, Wu MC, Shih HH, Zheng Q, et al. The empirical mode decomposition and the Hilbert spectrum for nonlinear and non-stationary time series analysis. Proc R Soc A Math Phys Eng Sci 1998;454:903–95. http://dx.doi.org/10.1098/rspa.1998.0193.
[49] Goncalves P, Rilling G, Flandrin P. On empirical mode decomposition and its algorithms. IEEE-EURASIP. Work Nonlinear Signal Image Process 2003;3:8–11. http://dx.doi.org/10.1109/ICASSP.2008.4518437.
[50] Feng S, Chen Q, Zuo C, Sun J, Tao T, Hu Y. A carrier removal technique for Fourier transform profilometry based on principal component analysis. Opt Lasers Eng 2015;74:80–6. http://dx.doi.org/10.1016/j.optlaseng.2015.05.009.
[51] Posdamer J, Altschuler M. Surface measurement by space-encoded projected beam systems. Comput Graph Image Process 1982;18:1–17. http://dx.doi.org/10.1016/0146-664X(82)90096-X.
[52] Sato K, Seiji I. Three-dimensional surface measurement by space encoding range imaging. J Robot Syst 2 1985;2:27–39.
[53] Hall-Holt O, Rusinkiewicz S. Stripe boundary codes for real-time structured-light range scanningof moving objects. Proc Eighth IEEE Int Conf Comput Vision ICCV 2001 2001. http://dx.doi.org/10.1109/ICCV.2001.937648.
[54] Rusinkiewicz S, Hall-Holt O, Levoy M. Real-time 3D model acquisition. ACM Trans Graph 2002:21. http://dx.doi.org/10.1145/566654.566600.
[55] Quan C, He XY, Wang C, Tay CJ, Shang HM. Shape measurement of small objects using LCD fringe projection with phase shifting. Opt Commun 2001;189:21–9.
[56] Huang PS, Zhang S. Fast three-step phase-shifting algorithm. Appl Opt 2006;45:5086–91. http://dx.doi.org/10.1364/AO.45.005086.
[57] Y. Hu J. Xi J. Chicharo Z. Yang, Improved three -step phase shifting profilometry using digital fringe pattern projection, In: Proceedings of the Computer Graphics Imaging Vision Technology Application, CGIV'06, vol. 2006, 2006, pp. 161–166, doi: 10.1109/CGIV.2006.58.
[58] Takasaki H. Moiré topography. Appl Opt 1970;9:1467–72.
[59] Benoit P, Mathieu E, Hormière J, Thomas A. Characterization and control of threedimensional objects using fringe projection techniques. Nouv Rev d'Optique 1975;6:67–86. http://dx.doi.org/10.1088/0335-7368/6/2/301.
[60] Pirodda L. Shadow and projection moire techniques for absolute or relative mapping of surface shapes. Opt Eng 1982;21:640–9. http://dx.doi.org/10.1117/12.7972959.
[61] Ryu W-J, Kang Y-J, Baik S-H, Kang S-J. A study on the 3-D measurement by using digital projection moiré method. Opt - Int J Light Electron Opt 2008;119:453–8. http://dx.doi.org/10.1016/j.ijleo.2006.12.016.
[62] Buytaert JAN, Dirckx JJJ. Moiré profilometry using liquid crystals for projection and demodulation. Opt Express 2008;16:179–93. http://dx.doi.org/10.1364/OE.16.000179.
[63] Dirckx JJJ, Buytaert JAN, Van der Jeught S. Implementation of phase-shifting moiré profilometry on a low-cost commercial data projector. Opt Lasers Eng 2010;48:244–50. http://dx.doi.org/10.1016/j.optlaseng.2009.03.013.
[64] Buytaert JAN, Dirckx JJJ. Phase-shifting Moiré topography using optical demodulation on liquid crystal matrices. Opt Lasers Eng 2010;48:172–81. http://dx.doi.org/10.1016/j.optlaseng.2009.03.018.

Please cite this article as: Van der Jeught S, Dirckx JJJ. Real-time structured light profilometry: a review. Opt Laser Eng (2016), http://dx.doi.org/10.1016/j.optlaseng.2016.01.011

[65] Engelhardt K. Acquisition of 3-D data by focus sensing utilizing the moire effect of CCD cameras. Appl Opt 1991;30:1401–7. http://dx.doi.org/10.1364/AO.30.001401.
[66] Zhang S, Huang P. High-Resolution, Real-time 3D Shape Acquisition. In: Proceedings of the 2004 Conference on Computer Vision and Pattern Recognition, Work 2004, doi:10.1109/CVPR.2004.86.
[67] Jia P, Kofman J, English C. Multiple-step triangular-pattern phase shifting and the influence of number of steps and pitch on measurement accuracy. Appl Opt 2007;46:3253–62. http://dx.doi.org/10.1364/AO.46.003253.
[68] Jia P, Kofman J, English C. Error compensation in two-step triangular-pattern phase-shifting profilometry. Opt Lasers Eng 2008;46:311–20. http://dx.doi.org/10.1016/j.optlaseng.2007.11.004.
[69] Zhang S, Yau S-T. High-speed three-dimensional shape measurement system using a modified two-plus-one phase-shifting algorithm. Opt Eng 2007;46:113603. http://dx.doi.org/10.1117/1.2802546.
[70] Wizinowich PL. Phase shifting interferometry in the presence of vibration: a new algorithm and system. Appl Opt 1990;29:3271–9. http://dx.doi.org/10.1364/AO.29.003271.
[71] Zuo C, Chen Q, Gu G, Feng S, Feng F. High-speed three-dimensional profilometry for multiply objects with complex shapes. Opt Express 2012;20:19493. http://dx.doi.org/10.1364/OE.20.019493.
[72] Ding Y, Xi J, Yu Y, Deng F. Absolute phase recovery of three fringe patterns with selected spatial frequencies. Opt Lasers Eng 2015;70:18–25. http://dx.doi.org/10.1016/j.optlaseng.2014.12.024.
[73] Zhang S. Recent progresses on real-time 3D shape measurement using digital fringe projection techniques. Opt Lasers Eng 2010;48:149–58. http://dx.doi.org/10.1016/j.optlaseng.2009.03.008.
[74] Wang Y, Zhang S, Oliver JH. 3D shape measurement technique for multiple rapidly moving objects. Opt Express 2011;19:8539–45. http://dx.doi.org/10.1364/OE.19.008539.
[75] Zhang S. Flexible 3D shape measurement using projector defocusing: extended measurement range. Opt Lett 2010;35:934–6. http://dx.doi.org/10.1364/OL.35.000934.
[76] Kim E-H, Hahn J, Kim H, Lee B. Profilometry without phase unwrapping using multi-frequency and four-step phase-shift sinusoidal fringe projection. Opt Express 2009;17:7818–30. http://dx.doi.org/10.1364/OE.17.007818.
[77] Wang Y, Zhang S. Superfast multifrequency phase-shifting technique with optimal pulse width modulation. Opt Express 2011;19:5149–55. http://dx.doi.org/10.1364/OE.19.005149.
[78] Karpinsky N, Hoke M, Chen V, Zhang S. High resolution, real-time three-dimensional shape measurement on graphics processing unit. Opt Eng 2014;53:024105.
[79] Lei Z, Wang C, Zhou C. Multi-frequency inverse-phase fringe projection profilometry for nonlinear phase error compensation. Opt Lasers Eng 2015;66:249–57. http://dx.doi.org/10.1016/j.optlaseng.2014.09.018.
[80] García-Isáis C a, Alcalá Ochoa N. One shot profilometry using a composite fringe pattern. Opt Lasers Eng 2014;53:25–30. http://dx.doi.org/10.1016/j.optlaseng.2013.08.006.
[81] García-Isáis CA, Alcalá Ochoa N. One shot profilometry using phase partitions. Opt Lasers Eng 2015;68:111–20. http://dx.doi.org/10.1016/j.optlaseng.2014.12.016.
[82] Guan C, Hassebrook L, Lau D. Composite structured light pattern for three-dimensional video. Opt Express 2003;11:406–17. http://dx.doi.org/10.1364/OE.11.000406.
[83] T.P. Koninckx I. Geys T. Jaeggli L. Van Gool A graph cut based adaptive structured light approach for real-time range acquisition. In: Proceedings of the 2nd International Symposium 3D Data Processing 2004 Visual Transm. 3DPVT, pp. 413–421, doi: 10.1109/TDPVT, 2004,1335268.
[84] Koninckx TP, Van Gool L. Real-time range acquisition by adaptive structured light. IEEE Trans Pattern Anal Mach Intell 2006;28:432–45. http://dx.doi.org/10.1109/TPAMI.2006.62.
[85] Koninckx TP, Griesser A, Van Gool L. Real-time range scanning of deformable surfaces by adaptively coded structured light. In: Proceedings of the Fourth International Conference on 3-D Digital Imaging Model 2003, 3DIM, 2003 Proceedings 2003, doi:10.1109/IM.2003.1240262.
[86] Griesser A, Koninckx TP, Van Gool L. Adaptive real-time 3D acquisition and contour tracking within a multiple structured light system. In: Proceedings of the 12th Pacific Conference on Computer Graphical Application, 2004, PG 2004, Proceedings 2004, pp. 361–70, doi:10.1109/PCCGA.2004.1348367.
[87] Zhao M, Huang L, Zhang Q, Su X, Asundi A, Kemao Q. Quality-guided phase unwrapping technique: comparison of quality maps and guiding strategies. Appl Opt 2011;50:6214–24.
[88] Lu Y, Wang X, Zhong X, He G, Liu Y, Zheng D. A new quality map for quality-guided phase unwrapping. Chin Opt Lett 2004;2:698–700.
[89] Su X. Reliability-guided phase unwrapping algorithm: a review. Opt Lasers Eng 2004;42:245–61. http://dx.doi.org/10.1016/j.optlaseng.2003.11.002.
[90] Herráez MA, Burton DR, Lalor MJ, Gdeisat MA. Fast two-dimensional phase-unwrapping algorithm based on sorting by reliability following a non-continuous path. Appl Opt 2002;41:7437–44.
[91] Zhang S, Li X, Yau S. Multilevel quality-guided phase unwrapping algori thm for real-time three-dimensional shape reconstruction. Appl Opt 2007;46:50–7.
[92] Nico G, Palubinskas G, Datcu M. Bayesian approaches to phase unwrapping: theoretical study. IEEE Trans Signal Process 2000:48. http://dx.doi.org/10.1109/78.863057.
[93] Marroquin JL, Tapia M, Rodriguez-Vera R, Servin M. Parallel algorithms for phase unwrapping based on Markov random field models. J Opt Soc Am A Opt Image Sci Vis 1995;12:2578–85.
[94] Xu W, Gumming L. A region-growing algorithm for InSAR phase unwrapping. IEEE Trans Geosci Remote Sens 1999;37:124–34. http://dx.doi.org/10.1109/36.739143.
[95] Schwartzkopf W, Milner TE, Ghosh J, Evans BL, Bovik a. C. Two-dimensional phase unwrapping using neural networks. Image Anal Interpret 2000 Proceedings 4th IEEE Southwest Symp 2000, pp. 274–7.
[96] Karout SA, Gdeisat MA, Burton DR, Lalor MJ. Two-dimensional phase unwrapping using a hybrid genetic algorithm. Appl Opt 2007;46:730–43. http://dx.doi.org/10.1364/AO.46.000730.
[97] Fornaro G, Franceschetti G, Lanari R. Interferometric SAR phase unwrapping using Green's formulation. IEEE Trans Geosci Remote Sens 1996;34:720–7. http://dx.doi.org/10.1109/36.499751.
[98] Suksmono AB, Hirose A. Improving phase-unwrapping result of InSAR images by incorporating the fractal model. Proc 2003 Int Conf Image Process (Cat No03CH37429) 2003;2. doi:10.1109/ICIP.2003.1246809.
[99] Carballo GF, Fieguth PW. Probabilistic cost functions for network flow phase unwrapping. IEEE Trans Geosci Remote Sens 2000;38:2192–201. http://dx.doi.org/10.1109/36.868877.
[100] Ghiglia DC, Mastin GA, Romero LA. Cellular-automata method for phase unwrapping. J Opt Soc Am A 1987;4:267–80.
[101] Ghiglia DC, Romero LA. Minimum L-p-norm two-dimensional phase unwrapping. J Opt Soc Am A 1996;13:1999. http://dx.doi.org/10.1364/JOSAA.13.001999.
[102] Chen CW, Zebker HA. Two-dimensional phase unwrapping with use of statistical models for cost functions in nonlinear optimization. J Opt Soc Am A 2001;18:338. http://dx.doi.org/10.1364/JOSAA.18.000338.
[103] Cusack R, Papadakis N. New robust 3-D phase unwrapping algorithms: application to magnetic field mapping and undistorting echoplanar images. Neuroimage 2002;16:754–64. http://dx.doi.org/10.1006/nimg.2002.1092.
[104] Jenkinson M. Fast, automated, N-dimensional phase-unwrapping algorithm. Magn Reson Med 2003;49:193–7. http://dx.doi.org/10.1002/mrm.10354.
[105] Van der Jeught S, Sijbers J, Dirckx J. Fast Fourier-based phase unwrapping on the graphics processing unit in real-time imaging applications. J Imaging 2015;1:31–44. http://dx.doi.org/10.3390/jimaging1010031.
[106] Read P, Meyer M-P. Restoration of motion picture film. Butterworth-Heinemann; 2000.
[107] Huang PS, Zhang C, Chiang F-P. High-speed 3-D shape measurement based on digital fringe projection. Opt Eng 2003;42:163. http://dx.doi.org/10.1117/1.1525272.
[108] Zhang S, High-resolution Huang P. real-time three-dimensional shape measurement. Opt Eng 2006;45:123601–8.
[109] Pan J, Huang PS, Zhang S, Chiang F-P. Color N-Ary Gray Code for 3-D Shape Measurement. ICEM12- 12th Int Conf Exp Mech 2004.
[110] Zhang S, Royer D, Yau S-T. GPU-assisted high-resolution, real-time 3-D shape measurement. Opt Express 2006;14:9120–9. http://dx.doi.org/10.1364/OE.14.009120.
[111] Liu K, Wang Y, Lau DL, Hao Q, Hassebrook LG. Dual-frequency pattern scheme for high-speed 3-D shape measurement. Opt Express 2010;18:5229–44. http://dx.doi.org/10.1364/OE.18.005229.
[112] Van der Jeught S, Soons J, Dirckx JJJ. Real-time microscopic phase-shifting profilometry. Appl Opt 2015;54:4953–9.
[113] Nguyen H, Nguyen D, Wang Z, Kieu H, Real-time Le M. High-accuracy 3D imaging and shape measurement. Appl Opt 2015. http://dx.doi.org/10.1364/ao.54.0000a9.
[114] G. Turk M. Levoy Zippered polygon meshes from range images. In: Proceedings of the 21st Annual Conference, 94, 1994 pp. 311–318, doi: 10.1145/192161.192241.
[115] Soucy M, Laurendeau D. Multi-resolution surface modeling from multiple range views. Proc 1992 IEEE comput soc conf comput vis. Pattern Recognit 1992. http://dx.doi.org/10.1109/CVPR.1992.223166.
[116] Han TD, Abdelrahman TS. HiCUDA: High-level GPGPU programming. IEEE Trans Parallel Distrib Syst 2011;23:78–90. http://dx.doi.org/10.1109/TPDS.2010.62.
[117] Gong Y, Zhang S. Ultrafast 3-D shape measurement with an off-the-shelf DLP projector. Opt Express 2010;18:19743–54.
[118] Su X-Y, Zhou W-S, von Bally G, Vukicevic D. Automated phase-measuring profilometry using defocused projection of a Ronchi grating. Opt Commun 1992;94:561–73. http://dx.doi.org/10.1016/0030-4018(92)90606-R.
[119] Lei S, Zhang S. Flexible 3-D shape measurement using projector defocusing. Opt Lett 2009;34:3080–2. http://dx.doi.org/10.1364/OL.34.003080.
[120] Takei J, Kagami S, Hashimoto K. 3,000-fps 3-D shape measurement using a high-speed camera–projector system. Discovery 2007:3211–6.
[121] Zhang S, Van Der Weide D, Oliver J. Superfast phase-shifting method for 3-D shape measurement. Opt Express 2010;18:9684–9. http://dx.doi.org/10.1364/OE.18.009684.
[122] Zuo C, Chen Q, Gu G, Feng S, Feng F, Li R, et al. High-speed three-dimensional shape measurement for dynamic scenes using bi-frequency tripolar pulse-width-modulation fringe projection. Opt Lasers Eng 2013;51:953–60. http://dx.doi.org/10.1016/j.optlaseng.2013.02.012.
[123] Gao W, Huyen NTT, Loi HS, Kemao Q. Real-time 2D parallel windowed Fourier transform for fringe pattern analysis using graphics processing unit. Opt Express 2009;17:23147–52. http://dx.doi.org/10.1364/OE.17.023147.

Please cite this article as: Van der Jeught S, Dirckx JJJ. Real-time structured light profilometry: a review. Opt Laser Eng (2016), http://dx.doi.org/10.1016/j.optlaseng.2016.01.011

[124] Chen L-C, Nguyen XL, Zhang F-H, Lin T-Y. High-speed Fourier transform profilometry for reconstructing objects having arbitrary surface colours. J Opt 2010;12:095502. http://dx.doi.org/10.1088/2040-8978/12/9/095502.
[125] Hu Y, Xi J, Li E, Chicharo J, Yang Z, Yu Y. A calibration approach for decoupling colour cross-talk using nonlinear blind signal separation network. Conf. Optoelectron. Microelectron. Mater. Devices, Proceedings, COMMAD, 2005, p. 265–8. doi:10.1109/COMMAD.2004.1577541.
[126] Hu Y, Xi J, Chicharo J, Yang Z. Blind color isolation for color-channel-based fringe pattern profilometry using digital projection. J Opt Soc Am A Opt Image Sci Vis 2007;24:2372–82. http://dx.doi.org/10.1364/JOSAA.24.002372.

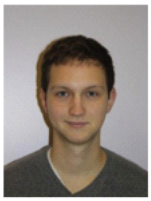

Sam Van der Jeught was born in Antwerp, Belgium, in 1987. He graduated as master in Physics in 2010 from the University of Antwerp, where he researched new ways of accelerating the digital signal processing algorithms involved in optical coherence tomography in a joint collaboration between the Laboratory of Biomedical Physics (BIMEF) and the University of Kent, UK. As a Marie Curie fellow, he was able to work at the Applied Optics Group (AOG) at the University of Kent for a period of 10 months. He received his degree of PhD in Science: Physics in 2015 at the University of Antwerp for the dissertation entitled "Optical techniques for real-time morphology measurement of the tympanic membrane". He is currently researching new optical methods for measuring human eardrum shape in real-time and in-vivo as a post-doctoral fellow with funding from the Research Foundation - Flanders (FWO).

Joris J.J. Dirckx was born in Antwerp , Belgium , in 1960. He graduated in Physics and in Didactics at the University of Antwerp , taught physics and mathematics in high school, and then became assistant at the University of Antwerp . In 1991 he obtained the PhD in Physics, with the dissertation "Automated moiré topography and its use for shape and deformation measurements of the eardrum". From 1992 to 1993 he worked as scientific advisor for the government (IWT), where he assessed and audited major industrial research projects, with a total project portfolio of over 10 million Euros. In 1994 he returned to research and worked at the ENT department of St. Augustinus hospital as clinical audiologist and performed research on oto-acoustic emissions and cochlear implants. In 1996 he joined the University of Antwerp as post-doc researcher, and was appointed lecturer in physics in 2000. He became professor in 2003, and is now director of the laboratory of Biomedical Physics and full professor in the Department of Physics. He teaches courses in general physics for pharmacy, biology and biochemistry students, physics of optical microscopy and courses in practical holography and biomedical imaging for physics students.

Please cite this article as: Van der Jeught S, Dirckx JJJ. Real-time structured light profilometry: a review. Opt Laser Eng (2016), http://dx.doi.org/10.1016/j.optlaseng.2016.01.011